THE JOURNAL OF PHYSICAL CHEMISTRY C

pubs.acs.org/JPCC Article

Electronic Descriptor of Single Metal-Oxo Species on Phthalocyanine- and Porphyrin-Functionalized Graphene toward Methane Activation Process

Dominick Filonowich, Miguel Luna, Thalia Quinn, and Pabitra Choudhury*

Cite This: J. Phys. Chem. C 2020, 124, 4502−4510 Read Online

ACCESS | Metrics & More | Article Recommendations | Supporting Information

ABSTRACT: Catalysts are needed to expedite methane-to-methanol conversion reactions by lowering the energy required for the reactions to produce high-value-added chemicals. In this work, single metal active site based on 10 different phthalocyanine-/porphyrin-functionalized graphene materials has been screened and characterized for the C−H bond activation of methane-to-methanol conversion process using ab initio density functional theory (DFT) calculations. The results show that a radical mechanism is the predominant mechanism for the C−H bond activation process of methane for these types of materials. An inverse correlation between the metal-oxo species formation energy and the C−H bond activation energy was observed, and both of them have a nice correlation with an electronic descriptor known as metal charge state of the metal-oxo species of these materials. The optimal performance of the catalysts can be attributed to the metal charge state value of the metal-oxo species, with an optimum value of 1.30 ± 0.03. Hence, the cobalt phthalocyanine-functionalized graphene (GCoPc) system seems to be a potential candidate for optimum utilization of energy for complete methane-to-methanol conversion process. The catalytic activity of this system can further be tuned by controlling the metal charge state of Co via both substrate doping and ligand exchange.

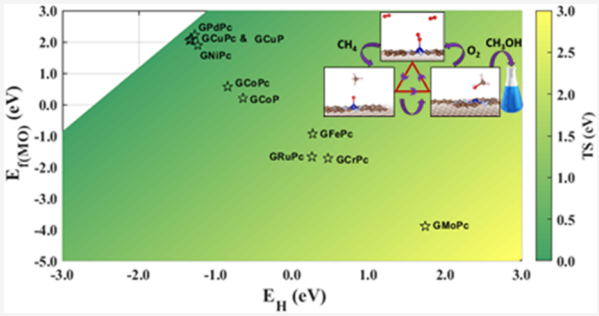

1. INTRODUCTION

Methane is the principal component in both shale gas and biogas but has low density. Hence, both storage and transportation are two major challenges for the methane economy. Therefore, methane to liquid fuel and/or chemical conversion has become a central research subject in modern chemistry. Moreover, industrial routes for conversion of methane to fuels and chemicals are limited because of the very highly stable tetrahedral C−H bonds that are weakly polarized. However, metal-oxo species can have the potential to break the C−H bonds of methane and convert it into methanol even at room temperature.[1,2] Our objective is to design a novel catalyst based on a single metal active center, which can convert methane to methanol with mild reaction conditions in a single-step process.[3] The single-step conversion process is thermodynamically more favorable than the two-step via synthesis gas (CO and H_2) process.

Many studies have been realized, both experimentally and theoretically, on methane catalytic conversion on single metal atoms anchored on various support materials ranging from metal oxides,[4−8] metal−organic frameworks (MOFs),[9−11] and zeolites[12−18] to carbonaceous materials such as nanotubes, fullerenes, and graphene.[19−27] On the other hand, macrocyclic molecules such as transition-metal phthalocyanines (TMPcs) and porphyrins are composed of a single metal atom and surrounding organic ligand rings. It has been shown that a combination of different transition-metal atoms and different substrate surfaces will lead to very different geometrical, electronic, catalytic, and magnetic properties.[28,29] The metal−ligand interaction and molecule−substrate interaction are the two most important parameters, which control the various physical and chemical properties of this self-assembled monolayer of macrocyclic molecules onto the substrate. Generally, these macrocyclic molecules provide a thermodynamically stable chemical environment for the central transition-metal atom. Recently, it was evidenced that these molecules have great potential in applications in catalysis.[29−32] It has been shown that copper-oxo species of copper porphyrin (CuP)-functionalized graphene is acting as the single-site active metal center for the methane catalytic oxidation.[33] This active center can facilitate methane adsorption and initiate the C−H bond activation and subsequent methanol formation process at very mild conditions. However, it has been observed from our theoretical results that the formation of metal-oxo

Received: September 12, 2019
Revised: January 24, 2020
Published: January 29, 2020

https://dx.doi.org/10.1021/acs.jpcc.9b08697
J. Phys. Chem. C 2020, 124, 4502−4510

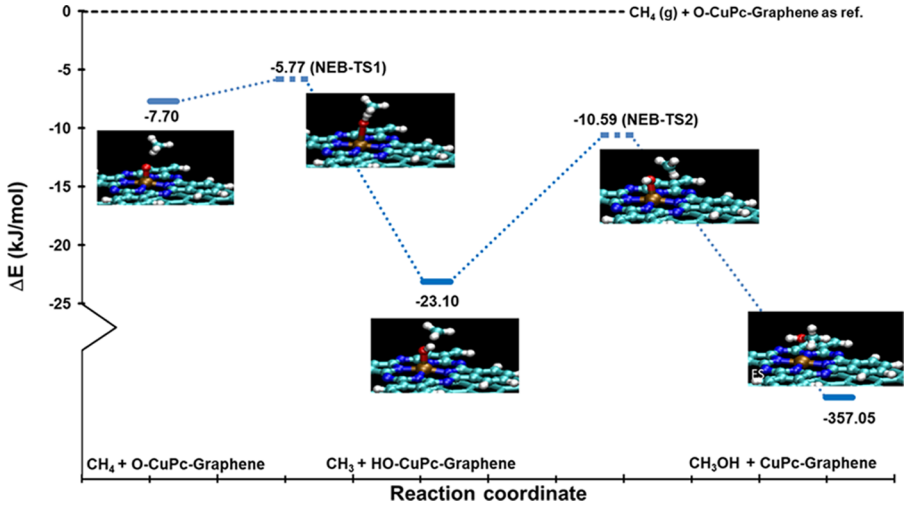

Figure 1. Reaction energy profile for the reaction of CH_4 with preadsorbed O atom on CuPc-functionalized graphene surface. The numbers indicate the energies relative to the reference system of gas-phase CH_4 and O bound to the metal center of the CuPc-functionalized graphene surface. The transition states are shown as the maxima on the energy landscapes. The *x*-axis corresponds to the reaction coordinate along the reaction pathway.

species on CuP-functionalized graphene has become a major challenge. This means that even though catalysts can break the C−H bond at a much lower temperature, they may not necessarily be an ideal candidate for complete methane-to-methanol conversion. The catalyst regeneration (i.e., oxo species formation on a single metal center) is another important step to be considered for the optimal single metal active site catalyst development.

In this work, we show that both the C−H bond activation and metal-oxo species formation on phthalocyanine- (TMPc) and porphyrin-functionalized graphene can be directly linked to electronic descriptors such as the metal charge state, active oxygen charge, and metal d-band center of metal-oxo species, and thereby an optimal single metal active catalysts can be screened for the methane-to-methanol conversion process. We have studied many different transition-metal phthalocyanine- (TMPc) and porphyrin-functionalized graphene, where TM = Fe, Ni, Co, Cu, Cr, Pd, Mo, and Ru atoms.

2. COMPUTATIONAL APPROACH

Spin-polarized periodic density functional theory (DFT) calculations were performed within the Perdew−Burke−Ernzerhof (PBE)[34] form of the generalized gradient approximation (GGA) implemented in the Vienna ab initio simulation package (VASP).[35,36] The projector-augmented wave method with an energy cutoff of 400 eV, including van der Waals (vdW) corrections, an efficient semiempirical scheme proposed by Grimme,[37] was applied to describe the interactions between valence electrons and frozen cores.[38] The electronic energies were converged to 10^{-6} using the Gaussian smearing method with a width of 0.1 eV around the Fermi level, which was applied to facilitate convergence. The ionic relaxations were performed until the residual forces between the atoms were within 20 meV/Å. The TMPc-functionalized graphene surface is periodic in the *x* and *y* directions with the dimensions of the supercell of 17.07 × 14.78 $Å^2$, and the *z* dimension of 25 Å was chosen to be large enough so that the interactions with periodic images were negligible. A 3 × 3 × 1 Monkhorst−Pack *k*-point mesh was used for sampling the Brillouin zone. We have used a quantitatively reasonable model for large supercells for our calculations based on experimental information[39−43] and our previous publications.[44,45] The C−H bond activation energy barriers were computed within DFT using the climbing image "nudged elastic band" (CI-NEB) method.[46−48] The detailed calculations and analysis methods have been discussed several times in our previous works.[32,33,44,49−51] It is to be noted that the catalytic reactions on transition metals may often occur through a spin-crossing mechanism, which can reduce the activation barriers. However, we have not used spin−orbit coupling (SOC) in this study to see if any spin crossing occurs. The detailed spin-crossing analysis to understand the effect of the spin crossing on energy barrier of the optimum catalyst is beyond the scope of this work.

3. RESULTS AND DISCUSSION

In the two-step methane-to-methanol conversion process, the initial step, homolytic C−H bond scission, is followed by methanol formation step via recombination of intermediates. Generally, there are two known possible mechanisms for the methane activation on the metal-oxo species on the phthalocyanine and porphyrin materials, namely, the direct-radical, and nonradical mechanisms. However, based on our previous results on copper-oxo species on CuP−O-functionalized graphene[33] and the energy landscapes of intermediates with energy barriers of FePc−O- and CuPc−O-functionalized graphene (as shown in Figures S1−S6 in the Supporting Information), it was observed that the radical mechanism would be the most predominant mechanism for the methane activation process for these types of materials. The complete radical reaction mechanism of methane activation on GCuPc−O and subsequent methanol formation step are shown in Figure 1. The results (Figure 1) clearly indicate that the active center (Cu−O) on GCuPc−O can facilitate methane adsorption and initiate the C−H bond activation and subsequent methanol formation process at very mild conditions, which is also consistent with the previous GCuP−O system.[33] Hence, the direct-radical mechanism has been considered for the rest of the analysis of other phthalocyanine and porphyrin materials in this work. However,

https://dx.doi.org/10.1021/acs.jpcc.9b08697
J. Phys. Chem. C 2020, 124, 4502−4510

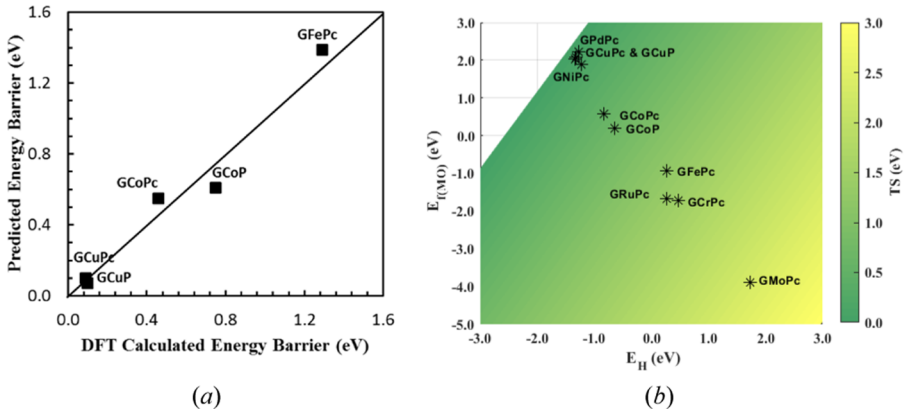

Figure 2. (a) Relationship between the transition-state energy (E_{TS}), calculated from the DFT−NEB method and predicted value from the catalyst's hydrogen affinity. (b) Relationship between the hydrogen abstraction energy (E_H), oxide formation energy ($E_{f(MO)}$), and transition-state energy (E_{TS}). Color bar is the scale for the transition-state energy. White area in the upper-left corner represents no energy barrier.

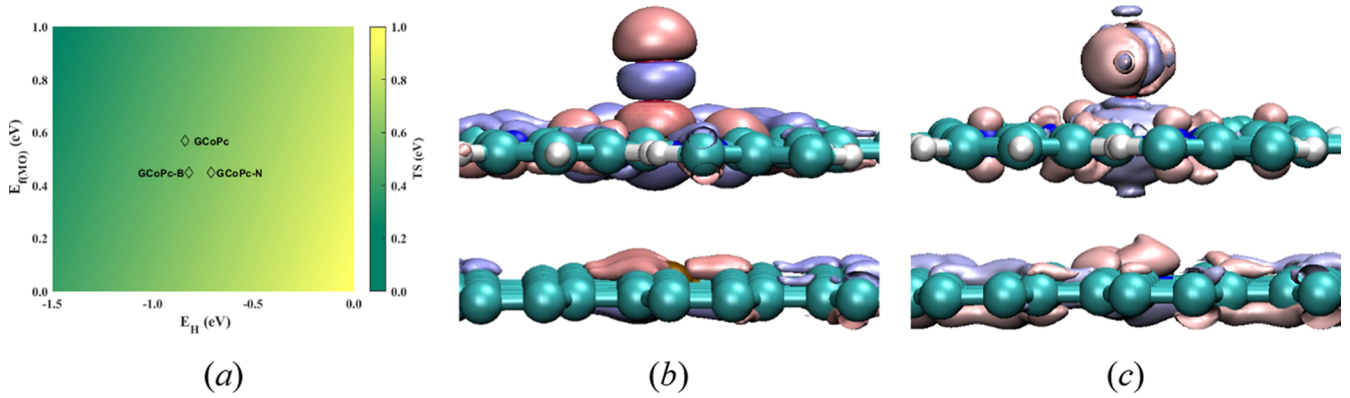

Figure 3. (a) Effect of N- and B-doping graphene substrates of GCoPc on the hydrogen abstraction energy (E_H), oxide formation energy ($E_{f(MO)}$), and transition-state energy (E_{TS}). Color bar is the scale for the transition-state energy. (b, c) Charge density difference plots between CoPc−O and graphene substrate with B and N dopings, respectively. The blue isosurface indicates the accumulated charge, and pink isosurface indicates the depletion charge. The isosurface values are 0.04027 and 0.03191e/Å^3, respectively, for B-doped and N-doped graphene substrates in the plot.

ideally one should analyze all of the transition-metal phthalocyanine catalysts to claim the previous statement, which, of course, takes enormous computational resources and time. Our objective is to quickly and also accurately screen the catalysts for the methane activation process via a radical mechanism based on fundamental electronic properties of a single structural configuration, single metal-oxo species on phthalocyanine-/porphyrin-functionalized graphene. Hence, the detailed structural analysis of various intermediates and reaction pathways is beyond the scope of this manuscript.

We have analyzed several single-atom active site catalysts based on transition-metal phthalocyanine- (TMPc) and porphyrin-functionalized graphene for the methane-to-methanol activation process. The transition-state energies for the methane activation process via radical mechanism of several systems (GCuPc−O, GFePc−O, GCoPc−O, GCoP−O and GCuP−O, as shown in Figures S1, S4, and S7−S9 in the Supporting Information) were calculated using expensive DFT−NEB simulations. We have then calculated these catalyst's hydrogen abstraction energies and subsequently predicted the transition-state energies using universal scaling relation[52] to compare and validate with the DFT−NEB calculated transition-state energies, as shown in Figure 2a. The hydrogen abstraction energy ($E_H = E_{f(MOH)} - E_{f(MO)}$) is defined as the difference between the formation energy of metal-OH and metal-oxo species on the phthalocyanine-/porphyrin-functionalized graphene surfaces. The formation energies for a given site were calculated relative to gas-phase O_2 and H_2O as given by the following equation

$$E_{f(MO_xH_y)} = E(GMPcO_xH_y) - \frac{y}{2}E(H_2O) - \left(\frac{x}{2} - \frac{y}{4}\right)E(O_2) - E(GMPc)$$

It can clearly be seen that the calculated transition-state energies from the DFT−NEB are well compared with the predicted transition-state energies. The calculated values, including the hydrogen abstraction energy and metal-oxo species formation energy, were then extended to other phthalocyanine and porphyrin materials and plotted against transition-state energies to determine the quality of each single-site active metal center catalyst, as shown in Figure 2b. It is to be noted that we used van der Waals-corrected spin-polarized periodic density functional theory (DFT) calculations to compute geometries, energetics, and reaction barriers for reactions on all of the model surfaces. For all of the states, the VASP optimizations automatically converged to the most stable spin state, which was confirmed by some additional calculations for three (Fe, Cu, and Mo) different phthalocyanine systems (as shown in Table S1 in the Supporting Information) with a fixed spin state other than the spin-

https://dx.doi.org/10.1021/acs.jpcc.9b08697
J. Phys. Chem. C 2020, 124, 4502−4510

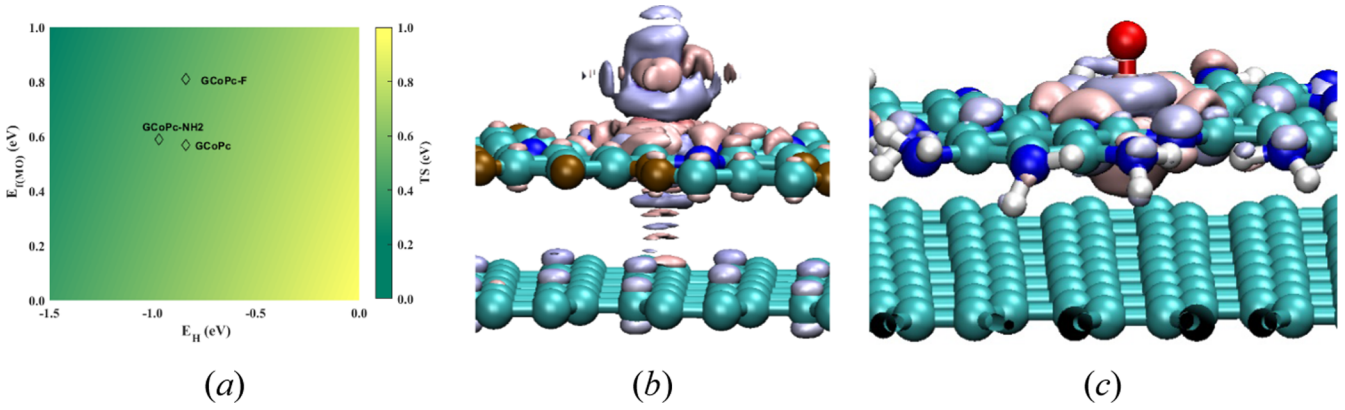

Figure 4. (a) Effect of F- and NH_2-ligand exchanges of phthalocyanine of the GCoPc surface on the hydrogen abstraction energy (E_H), oxide formation energy ($E_{f(MO)}$), and transition-state energy (E_{TS}). Color bar is the scale for the transition-state energy. (b, c) Charge density difference plots between graphene substrate and F- and NH_2-ligand exchanges of CoPc−O, respectively. The blue isosurface indicates the accumulated charge, and pink isosurface indicates the depletion charge. The isosurface values are 0.03148 and 0.03189e/Å^3, respectively, for F-ligand and NH_2-ligand phthalocyanines in the plot.

polarized VASP-converged ground-state configuration. This means that the oxo species formation energies and H-abstraction energies were the results of the difference between the reactants and products with reference to their most stable spin state configurations. Hence, both the oxo species formation and H-abstraction energies were assumed to be the correct values leading to prediction of energy barriers with reasonable accuracy to quickly identify the optimum catalyst.

It can be clearly seen in Figure 2b that we have a negative correlation between the hydrogen affinity and the oxide formation energy ($E_{f(MO)}$) for each catalyst. It has also been observed that despite the low transition-state energies (i.e., high C−H bond activation reaction rate) provided by the copper-, palladium-, and nickel-based catalysts, each of them has a large oxide formation energy (Figure 2b). On the contrary, the molybdenum-based catalyst, which possesses the lowest oxide formation energy, has the highest transition-state energy, which is unfavorable for C−H bond activation. Cobalt phthalocyanine-functionalized graphene (GCoPc) and cobalt porphyrin-functionalized graphene (GCoP) are predicted to be the optimal catalysts among all of the catalysts that we have screened based on both the two key parameters (i.e., catalyst's ability to break the C−H bonds or C−H bond activation and its regeneration or metal-oxo species formation). We have further studied the effect of substrate doping and changing the pthalocyanine ligands on both metal-oxo species formation energy and the C−H bond activation process of the optimum catalyst, the GCoPc system. It is also to be noted that the white area in the upper-left corner of Figure 2b represents no energy barrier for the C−H bond activation process, i.e., spontaneous reaction.

3.1. Substrate Doping of GCoPc. We have studied the effect of N- and B-doped graphene substrates (as shown in Figure S10a,b in the Supporting Information) on both the metal-oxo species formation energy and the C−H bond activation process of the GCoPc system, as shown in Figure 3a. Looking at the Bader charge analysis of cobalt-oxo species on GCoPc, the pristine graphene substrate acts as a Lewis acid (electron acceptor) with an electron deficiency of 0.035e. The N-doped graphene substrate also acts as a Lewis acid with an electron deficiency of 0.113e, whereas the B-doped substrate acts as a Lewis base (electron donator) with an electron excess of 0.049e, which can also be seen from the charge density difference calculations for the B- and N-doped substrates of the GCoPc−O system, as shown in Figure 3b,c, respectively. The nitrogen-doped substrate increases the hydrogen abstraction energy, while favorable toward the metal-oxo species formation energy, and thereby increases the C−H bond activation energy from the nondoping by about 0.10 eV. The boron-doped substrate acts as a Lewis base and is favorable toward the metal-oxo species formation energy, while having a very small impact on the hydrogen abstraction energy, ultimately very slightly increasing the C−H bond activation energy by 0.02 eV.

3.2. Ligand Exchange of GCoPc. We have also studied the effect of F- and NH_2-ligand exchanges of phthalocyanine (as shown in Figure S10c,d in the Supporting Information) on both metal-oxo species formation energy and the C−H bond activation process of the GCoPc system, as shown in Figure 4a. From the charge analysis, it can be seen that the F-ligand exchange of phthalocyanine also causes the substrate to act as a Lewis base with an electron excess of 0.445e, whereas the NH_2-ligand exchange of phthalocyanine causes the substrate to act as a Lewis acid with an electron deficiency of 1.034e, which can also be seen from the charge density difference calculations for the F- and NH_2-ligand exchanges of the GCoPc−O system, as shown in Figure 4b,c, respectively. The F-ligand exchange has almost no impact on the hydrogen abstraction energy while being unfavorable toward the metal-oxo species formation energy, and therefore it does not have a significant impact on the C−H bond activation energy. On the contrary, the NH_2-ligand exchange of phthalocyanine has a lesser effect on the metal-oxo species formation energy, while being much more favorable toward hydrogen abstraction energy, therefore lowering the C−H bond activation energy by 0.10 eV.

Based on the current results, it can be concluded that substrate doping and ligand exchange can be used to further tune the reactivity of the GCoPc catalyst toward methane-to-methanol conversion process. Moreover, doping elements that causes the substrate to become Lewis base has a favorable effect toward metal-oxo species formation energy but has less effect on C−H bond activation energy. On the contrary, ligands that cause the substrate to become Lewis acid has a favorable effect toward C−H bond activation energy but has a negligible effect on metal-oxo species formation energy. Hence, B-doping graphene substrate and NH_2 ligand seem to be the preferable choice for the tuning of the GCoPc catalyst.

https://dx.doi.org/10.1021/acs.jpcc.9b08697
J. Phys. Chem. C 2020, 124, 4502−4510

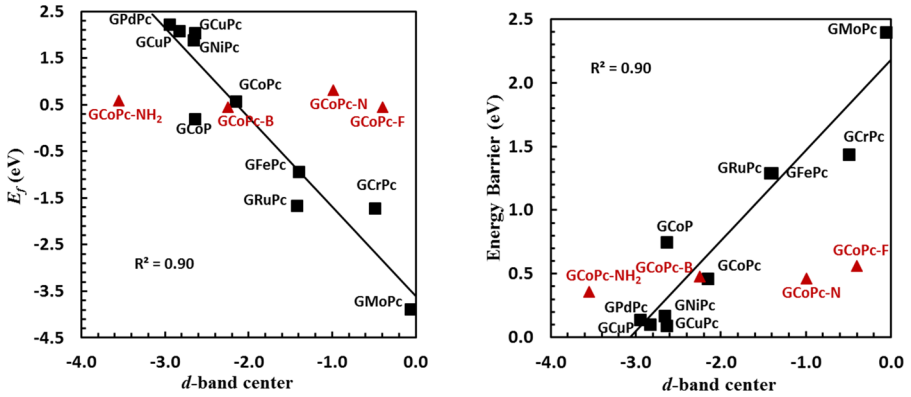

Figure 5. (a) Metal d-band center of the catalyst explored as a descriptor of metal-oxo species formation energy, E_f. (b) Metal d-band center of the catalyst explored as a descriptor of C−H bond activation energy. Zero energy scale on the *x*-axis is referenced to the Fermi surface. Black squares represent the GTMPc−O systems, and red triangles represent the GCoPc−O system with graphene substrate modified with N and B dopings, and CoPc with NH_2 and F ligands.

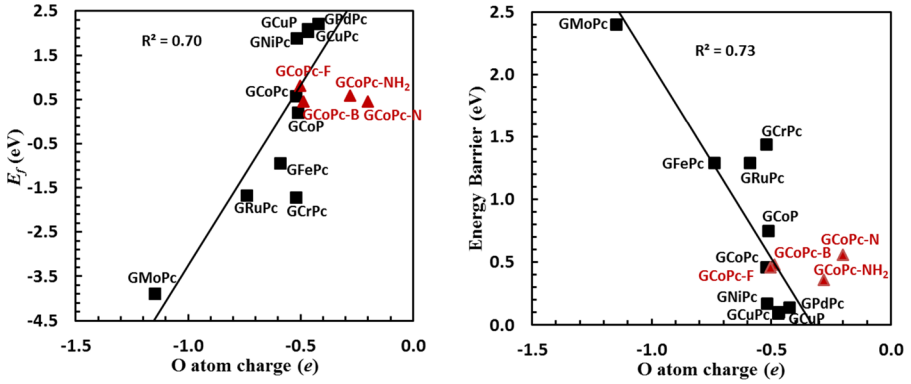

Figure 6. Dependency of (a) metal-oxo species formation energy, E_f, and (b) C−H bond activation energy barrier on O atom charge of catalysts. Black squares represent the GTMPc−O systems, and red triangles represent the GCoPc−O system with graphene substrate modified with N and B dopings, and CoPc with NH_2 and F ligands.

3.3. Electronic Descriptors. *3.3.1. Metal d-Band Center.*

The catalysts were further analyzed to understand the descriptor(s) based on the electronic properties of the single metal-oxo species on phthalocyanine/porphyrin materials. We initially used the metal d-band center of the single metal-oxo species as an electronic descriptor of both the metal-oxo species formation energy and C−H bond activation energy barrier. We have calculated the metal d-band center[53] from partial density of state calculations of metal-oxo species of all of the catalysts and plotted against the calculated metal-oxo species formation energy and predicted C−H bond activation energy barrier. The results are shown in Figure 5.

It can be seen from Figure 5 that the Mo system has a d-band center value of −0.06 eV closest to the Fermi surface, and the Pd system has a d-band center value of −2.9 eV farthest away from the Fermi surface. The metal d-band center of the metal-oxo systems in increasing order is as follows: GMoPc < GCrPc < GFePc < GRuPc < GCoPc < GCoP < GCuPc < GNiPc < GCuP < GPdPc. The metal-oxo bond formation and its catalytic function are dependent on the occupation of the d-orbitals.[54] The closer the metal d-band center is relative to the Fermi surface; the stored energy in the M−O bond is increased,[55] thereby forming a stronger M−O bond, and hence easier to form a very stable metal-oxo complex. The Mo, Cr, Fe, and Ru systems have a d-band center closer to the Fermi surface, and this allows for the systems to form a metal-oxo bond in a thermodynamically favorable way, which may be due to the lower electron affinity. So, the trend observed in Figure 5a is consistent with the fact that the metal d-band center nearer to the Fermi surface supports oxide formation. On the contrary, the d-band center (as shown in Figure 5b) of metal-oxo species is relative to the Fermi surface, the trend is flipped with reference to the C−H bond activation process.

3.3.2. Active O Atom Charge. It was previously reported that the charge of reactive O on the active site may influence C−H bond activation.[56,57] Hence, we also performed Bader charge analysis on active O atom of each metal-oxo species and plotted against both the metal-oxo species formation energy and C−H bond activation energy barrier, as shown in Figure 6.

It has been found that Cu-, Pd-, and Ni-based systems have lower excess electrons on the O atom (as shown in Figure 6) as compared to the Mo-, Cr-, Fe-, and Ru-based systems. Charge analysis clearly indicates that the metal-oxo species with lower excess electron on O atom has a higher capability to attract H atom from the C−H bond of methane and hence better is the C−H bond reactivity, consistent with the previous trend of d-band center (Figure 5b).

https://dx.doi.org/10.1021/acs.jpcc.9b08697
J. Phys. Chem. C 2020, 124, 4502−4510

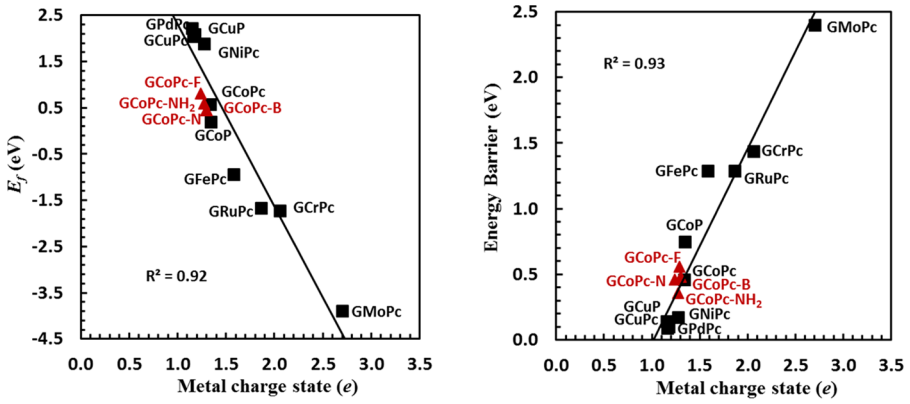

Figure 7. (a) Metal charge state of a catalyst explored as a descriptor of metal-oxo species formation energy, E_f. (b) Metal charge state of a catalyst explored as a descriptor of C−H bond activation energy. Black squares represent the GTMPc−O systems, and red triangles represent the GCoPc−O system with graphene substrate modified with N and B dopings, and CoPc with NH_2 and F ligands.

It is, however, very important to note that the electronic descriptors based on metal d-band center and charge on the reactive O atom of the reactive center do not represent the trend with a clear correlation with both the metal-oxo species formation energy and C−H bond activation energy for the methane activation process. Especially, in the case of substrate doping and ligand exchange, the correlations are even worse, as shown by the red triangles in Figures 5 and 6. It is, however, to be pointed out that both the substrate doping and ligand exchange did not break away from the correlation between metal-oxo formation and hydrogen abstraction energy for these materials, as shown in Figure S11 in the Supporting Information. Hence, expensive NEB calculations were not performed.

3.3.3. Metal Charge State. We also then analyzed the metal charge state of each catalyst, considered as another potential electronic descriptor, by defining the change in valence electrons when forming bond(s) from its original state after the relaxation and then plotted against the same metal-oxo species formation energy and C−H bond activation energy barrier, as shown in Figure 7.

It can clearly be seen from Figure 7 that the Mo system has the highest charge state value of 2.70, and the Pd system has the lowest charge state value of 1.15. The metal charge state of the metal-oxo systems in decreasing order is as follows: GMoPc > GCrPc > GRuPc > GFePc > GCoP > GCoPc > GNiPc > GCuP > GCuPc > GPdPc. Both the metal-oxo bond formation and its catalytic function are clearly dependent on the charge state of the single-atom active metal center, as can be seen from Figure 7. The metal charge state (GPdPc, GCuPc, GCuP, and GNiPc) is lower, clearly favoring the C−H bond activation while being quite challenging toward the metal-oxo species formation energy. In other words, the highest metal charge state of the GMoPc system will be the most favorable toward metal-oxo bond formation, whereas the same system will have the highest energy barrier for the C−H bond scission. GCoPc and GCoP are predicted to be the optimal catalysts that have the metal charge state values of 1.33 and 1.34, respectively. Overall, the trend observed in Figure 7 is consistent with the trends observed in both Figures 5 and 6. Moreover, the new electronic descriptor based on the metal charge state of the reactive center including substrate doping and ligand exchange does represent the trend with a clear correlation with both the metal-oxo species formation energy and C−H bond activation energy for the methane activation process. It is important to note that the metal charge states on the metal center of metal-oxo systems are not similar to on their common oxides, and this could be due to the different local environment created by various organic linkers/ligands in metal−organic systems.[58−60]

4. CONCLUSIONS

We used density functional theory to screen a variety of single metal atom active catalysts, and transition-metal phthalocyanine- (TMPc) and porphyrin-functionalized graphene for the C−H bond activation and, more specifically, the methane-to-methanol conversion process. It has been observed that the metal-oxo species, the active center for methane oxidation process, on metal phthalocyanine-/porphyrin-functionalized graphene can be created at reasonable temperatures. These single metal-oxo centers can be utilized to activate the C−H bond of methane at much lower temperatures than that of industrial processes. We have tried to identify by screening these single metal atom centers for both the reactivity toward C−H activation and catalyst activation at low-temperature conditions. We observed that Mo, Cr, Fe, and Ru systems have a high energy barrier for C−H bond activation but favorable metal-oxo species formation energy. On the contrary, Cu-, Pd-, and Ni-based systems have high energy demand for metal-oxo species formation to activate the catalyst but very low energy barrier for C−H bond activation. Both these characteristics (metal-oxo species formation and hydrogen abstraction energy) can be attributed to the metal charge state of the metal-oxo species of phthalocyanine/porphyrin materials. A metal charge state value of near 1.30 ± 0.03 could be an ideal choice for optimal single metal atom catalyst design for methane-to-methanol conversion process. The GCoPc system seems to be a potential candidate for optimum utilization of energy for complete methane to liquid fuel/chemical conversion process. The catalytic activity of GCoPc can then be further tuned by controlling the metal charge state of the Co metal atom via both substrate doping and ligand exchange, which influence the complete methane-to-methanol conversion process. It is important to note that the overoxidation of methane on the catalyst surface is an important concern toward selective methane-to-methanol conversion process for

https://dx.doi.org/10.1021/acs.jpcc.9b08697
J. Phys. Chem. C 2020, 124, 4502−4510

the practical applications. It has been recently shown that Co-oxo species can be created over Co/Gr surface by oxidizing the catalyst surface by N_2O. The reaction mechanism of different oxidative products, including methanol, carbene, and methyl radical, has been studied on this surface and found that the reaction rate producing methanol is much faster than producing the other products.[61] We would also expect the high activity and selectivity toward methanol formation on the GCoPc/graphene catalyst using N_2O as an oxidizing agent. Another combined theoretical and experimental study showed that Fe−O species can be created over graphene-confined single Fe atoms (FeN_4/graphene) by oxidizing with H_2O_2 and observed that methane conversion proceeds on the O−FeN_4−O active site along a radical pathway to produce CH_3OH and CH_3OOH first, and then the generated CH_3OH can be further catalyzed to form $HOCH_2OOH$ and HCOOH at room temperature.[62] It can be concluded that the C−H bond activation of methane is the rate-limiting step in the process of converting methane to a valuable liquid feedstock at low temperature, which is of practical importance. Another point observed is that the overoxidation of methane depends on the oxidizing agent used to create the metal-oxo complex. It would be interesting to see if changing the oxidizing agent or controlling the concentration of an oxidizing agent has a different effect on the methanol selectivity during the methane oxidation process. However, this is beyond the scope of this manuscript. This would be discussed in future work.

■ ASSOCIATED CONTENT

Supporting Information

The Supporting Information is available free of charge at https://pubs.acs.org/doi/10.1021/acs.jpcc.9b08697.

Energy landscapes of homolytic C−H bond scission with energy barriers of GCuPc−O, GFePc−O, GCoPc−O, GCoP−O, and GCuP−O; B- and N-doped graphene substrates of CoPc/graphene structures; F- and NH_2-ligand exchanges of CoPc/graphene structures; inverse relationship between the hydrogen abstraction energy (E_H) and metal-oxo species formation energy ($E_{f(MO)}$) w.r.t. the transition-state energy (E_{TS}); metal charge state as a descriptor of metal-oxo species formation energy, E_f; and C−H bond activation energies of simultaneous B-doped and NH_2-ligand exchanges of the GCoPc−O system (PDF)

■ AUTHOR INFORMATION

Corresponding Author

Pabitra Choudhury − *Chemical Engineering Department and Materials Engineering Department, New Mexico Tech, Socorro, New Mexico 87801, United States;* orcid.org/0000-0002-5023-9154; Email: pabitra.choudhury@nmt.edu

Authors

Dominick Filonowich − *Chemical Engineering Department, New Mexico Tech, Socorro, New Mexico 87801, United States*

Miguel Luna − *Chemical Engineering Department, New Mexico Tech, Socorro, New Mexico 87801, United States*

Thalia Quinn − *Chemical Engineering Department, New Mexico Tech, Socorro, New Mexico 87801, United States*

Complete contact information is available at: https://pubs.acs.org/10.1021/acs.jpcc.9b08697

Notes

The authors declare no competing financial interest.

■ ACKNOWLEDGMENTS

Acknowledgment is made to the Donors of the American Chemical Society Petroleum Research Fund (ACS-PRF, 58740-UR6) for support of this research. This work used the Extreme Science and Engineering Discovery Environment (XSEDE), which is supported by National Science Foundation grant number ACI-1548562, TACC at the stampede2 through allocation [TG-DMR140131]. Use of the Center for Nanoscale Materials was supported by the U.S. Department of Energy, Office of Science, Office of Basic Energy Sciences, under Contract No. DE-AC02-06CH11357.

■ REFERENCES

(1) Schroeder, D.; Fiedler, A.; Hrusak, J.; Schwarz, H. Experimental and Theoretical Studies toward a Characterization of Conceivable Intermediates Involved in the Gas-Phase Oxidation of Methane by Bare Feo^+. Generation of Four Distinguishable $[Fe,C,H_4,O]^+$ Isomers. *J. Am. Chem. Soc.* **1992**, *114*, 1215−1222.

(2) Baik, M.-H.; Newcomb, M.; Friesner, R. A.; Lippard, S. J. Mechanistic Studies on the Hydroxylation of Methane by Methane Monooxygenase. *Chem. Rev.* **2003**, *103*, 2385−2420.

(3) Shilov, A. E.; Shul'pin, G. B. Activation of C−H Bonds by Metal Complexes. *Chem. Rev.* **1997**, *97*, 2879−2932.

(4) Flytzani-Stephanopoulos, M.; Gates, B. C. Atomically Dispersed Supported Metal Catalysts. *Annu. Rev. Chem. Biomol. Eng.* **2012**, *3*, 545−574.

(5) Yi, N.; Saltsburg, H.; Flytzani-Stephanopoulos, M. Hydrogen Production by Dehydrogenation of Formic Acid on Atomically Dispersed Gold on Ceria. *ChemSusChem* **2013**, *6*, 816−819.

(6) Walker, J. M.; Gou, L.; Bhattacharyya, S.; Lindahl, S. E.; Zaleski, J. M. Photothermal Plasmonic Triggering of Au Nanoparticle Surface Radical Polymerization. *Chem. Mater.* **2011**, *23*, 5275−5281.

(7) Qiao, B.; Wang, A.; Yang, X.; Allard, L. F.; Jiang, Z.; Cui, Y.; Liu, J.; Li, J.; Zhang, T. Single-Atom Catalysis of Co Oxidation Using Pt_1/Feo_x. *Nat. Chem.* **2011**, *3*, 634−641.

(8) Gole, J. L.; White, M. G. Nanocatalysis: Selective Conversion of Ethanol to Acetaldehyde Using Mono-Atomically Dispersed Copper on Silica Nanospheres. *J. Catal.* **2001**, *204*, 249−252.

(9) Mulfort, K. L.; Farha, O. K.; Stern, C. L.; Sarjeant, A. A.; Hupp, J. T. Post-Synthesis Alkoxide Formation within Metal−Organic Framework Materials: A Strategy for Incorporating Highly Coordinatively Unsaturated Metal Ions. *J. Am. Chem. Soc.* **2009**, *131*, 3866−3868.

(10) Himsl, D.; Wallacher, D.; Hartmann, M. Improving the Hydrogen-Adsorption Properties of a Hydroxy-Modified Mil-53(Al) Structural Analogue by Lithium Doping. *Angew. Chem., Int. Ed.* **2009**, *48*, 4639−4642.

(11) Cohen, S. M. Postsynthetic Methods for the Functionalization of Metal−Organic Frameworks. *Chem. Rev.* **2012**, *112*, 970−1000.

(12) Kaminski, P.; Sobczak, I.; Decyk, P.; Ziolek, M.; Roth, W. J.; Campo, B.; Daturi, M. Zeolite MCM-22 Modified with Au and Cu for Catalytic Total Oxidation of Methanol and Carbon Monoxide. *J. Phys. Chem. C* **2013**, *117*, 2147−2159.

(13) Gruenert, W.; Hayes, N. W.; Joyner, R. W.; Shpiro, E. S.; Siddiqui, M. R. H.; Baeva, G. N. Structure, Chemistry, and Activity of Cu-ZSM-5 Catalysts for the Selective Reduction of Nox in the Presence of Oxygen. *J. Phys. Chem. A* **1994**, *98*, 10832−10846.

(14) Bayram, E.; Lu, J.; Aydin, C.; Uzun, A.; Browning, N. D.; Gates, B. C.; Finke, R. G. Mononuclear Zeolite-Supported Iridium: Kinetic, Spectroscopic, Electron Microscopic, and Size-Selective Poisoning Evidence for an Atomically Dispersed True Catalyst at 22 °C. *ACS Catal.* **2012**, *2*, 1947−1957.

(15) Bordiga, S.; Groppo, E.; Agostini, G.; van Bokhoven, J. A.; Lamberti, C. Reactivity of Surface Species in Heterogeneous Catalysts

Probed by in Situ X-Ray Absorption Techniques. *Chem. Rev.* **2013**, *113*, 1736−1850.
(16) Hammond, C.; et al. Aqueous-Phase Methane Oxidation over Fe-MFI Zeolites; Promotion through Isomorphous Framework Substitution. *ACS Catal.* **2013**, *3*, 1835−1844.
(17) Wulfers, M. J.; Teketel, S.; Ipek, B.; Lobo, R. F. Conversion of Methane to Methanol on Copper-Containing Small-Pore Zeolites and Zeotypes. *Chem. Commun.* **2015**, *51*, 4447−4450.
(18) Hammond, C.; Forde, M. M.; Rahim, A.; Hasbi, M.; Thetford, A.; He, Q.; Jenkins, R. L.; Dimitratos, N.; Lopez-Sanchez, J. A.; Dummer, N. F.; et al. Direct Catalytic Conversion of Methane to Methanol in an Aqueous Medium by Using Copper-Promoted Fe-ZSM-5. *Angew. Chem., Int. Ed.* **2012**, *51*, 5129−5133.
(19) Wang, H.; et al. Doping Monolayer Graphene with Single Atom Substitutions. *Nano Lett.* **2012**, *12*, 141−144.
(20) Kochubey, D. I.; Chesnokov, V. V.; Malykhin, S. E. Evidence for Atomically Dispersed Pd in Catalysts Supported on Carbon Nanofibers. *Carbon* **2012**, *50*, 2782−2787.
(21) Wang, Y.; Li, A.; Wang, K.; Guan, C.; Deng, W.; Li, C.; Wang, X. Reversible Hydrogen Storage of Multi-Wall Carbon Nanotubes Doped with Atomically Dispersed Lithium. *J. Mater. Chem.* **2010**, *20*, 6490−6494.
(22) Wang, H.; Feng, Q.; Cheng, Y.; Yao, Y.; Wang, Q.; Li, K.; Schwingenschlögl, U.; Zhang, X. X.; Yang, W. Atomic Bonding between Metal and Graphene. *J. Phys. Chem. C* **2013**, *117*, 4632−4638.
(23) Krasheninnikov, A. V.; Lehtinen, P. O.; Foster, A. S.; Pyykkö, P.; Nieminen, R. M. Embedding Transition-Metal Atoms in Graphene: Structure, Bonding, and Magnetism. *Phys. Rev. Lett.* **2009**, *102*, No. 126807.
(24) Wannakao, S.; Nongnual, T.; Khongpracha, P.; Maihom, T.; Limtrakul, J. Reaction Mechanisms for Co Catalytic Oxidation by N_2O on Fe-Embedded Graphene. *J. Phys. Chem. C* **2012**, *116*, 16992−16998.
(25) Janthon, P.; Viñes, F.; Kozlov, S. M.; Limtrakul, J.; Illas, F. Theoretical Assessment of Graphene-Metal Contacts. *J. Chem. Phys.* **2013**, *138*, No. 244701.
(26) Yang, X.-F.; Wang, A.; Qiao, B.; Li, J.; Liu, J.; Zhang, T. Single-Atom Catalysts: A New Frontier in Heterogeneous Catalysis. *Acc. Chem. Res.* **2013**, *46*, 1740−1748.
(27) Impeng, S.; Khongpracha, P.; Warakulwit, C.; Jansang, B.; Sirijaraensre, J.; Ehara, M.; Limtrakul, J. Direct Oxidation of Methane to Methanol on Fe-O Modified Graphene. *RSC Adv.* **2014**, *4*, 12572−12578.
(28) Hu, Z.; Li, B.; Zhao, A.; Yang, J.; Hou, J. G. Electronic and Magnetic Properties of Metal Phthalocyanines on Au(111) Surface: A First-Principles Study. *J. Phys. Chem. C* **2008**, *112*, 13650−13655.
(29) Sorokin, A. B. Phthalocyanine Metal Complexes in Catalysis. *Chem. Rev.* **2013**, *113*, 8152−8191.
(30) Sorokin, A. B.; Kudrik, E. V. Phthalocyanine Metal Complexes: Versatile Catalysts for Selective Oxidation and Bleaching. *Catal. Today* **2011**, *159*, 37−46.
(31) Kudrik, E. V.; Safonova, O.; Glatzel, P.; Swarbrick, J. C.; Alvarez, L. X.; Sorokin, A. B.; Afanasiev, P. Study of N-Bridged Diiron Phthalocyanine Relevant to Methane Oxidation: Insight into Oxidation and Spin States from High Resolution 1s Core Hole X-Ray Spectroscopy. *Appl. Catal., B* **2012**, *113*−*114*, 43−51.
(32) Mussell, S.; Choudhury, P. Density Functional Theory Study of Iron Phthalocyanine Porous Layer Deposited on Graphene Substrate: A Pt-Free Electrocatalyst for Hydrogen Fuel Cells. *J. Phys. Chem. C* **2016**, *120*, 5384−5391.
(33) Quinn, T.; Choudhury, P. Direct Oxidation of Methane to Methanol on Single-Site Copper-Oxo Species of Copper Porphyrin Functionalized Graphene: A DFT Study. *Mol. Catal.* **2017**, *431*, 9−14.
(34) Perdew, J. P.; Burke, K.; Ernzerhof, M. Generalized Gradient Approximation Made Simple. *Phys. Rev. Lett.* **1996**, *77*, No. 3865.
(35) Kresse, G.; Furthmüller, J. Efficiency of Ab-Initio Total Energy Calculations for Metals and Semiconductors Using a Plane-Wave Basis Set. *Comput. Mater. Sci.* **1996**, *6*, 15−50.
(36) Kresse, G.; Hafner, J. Ab Initio Molecular Dynamics for Liquid Metals. *Phys. Rev. B* **1993**, *47*, No. 558.
(37) Grimme, S. Semiempirical GGA-Type Density Functional Constructed with a Long-Range Dispersion Correction. *J. Comput. Chem.* **2006**, *27*, 1787−1799.
(38) Kresse, G.; Joubert, D. From Ultrasoft Pseudopotentials to the Projector Augmented-Wave Method. *Phys. Rev. B* **1999**, *59*, No. 1758.
(39) Tanaka, Y.; Mishra, P.; Tateishi, R.; Cuong, N. T.; Orita, H.; Otani, M.; Nakayama, T.; Uchihashi, T.; Sakamoto, K. Highly Ordered Cobalt−Phthalocyanine Chains on Fractional Atomic Steps: One-Dimensionality and Electron Hybridization. *ACS Nano* **2013**, *7*, 1317−1323.
(40) Ishida, N.; Fujita, D. Adsorption of Co-Phthalocyanine on the Rutile TiO_2(110) Surface: A Scanning Tunneling Microscopy/Spectroscopy Study. *J. Phys. Chem. C* **2012**, *116*, 20300−20305.
(41) Wießner, M.; Kübert, J.; Feyer, V.; Puschnig, P.; Schöll, A.; Reinert, F. Lateral Band Formation and Hybridization in Molecular Monolayers: NTCDA on Ag(110) and Cu(100). *Phys. Rev. B* **2013**, *88*, No. 075437.
(42) Liu, X.; Wei, Y.; Reutt-Robey, J. E.; Robey, S. W. Dipole−Dipole Interactions in TiOPc Adlayers on Ag. *J. Phys. Chem. C* **2014**, *118*, 3523−3532.
(43) Huang, H.; Wong, S. L.; Chen, W.; Wee, A. T. S. LT-STM Studies on Substrate-Dependent Self-Assembly of Small Organic Molecules. *J. Phys. D: Appl. Phys.* **2011**, *44*, No. 464005.
(44) Park, J. H.; Choudhury, P.; Kummel, A. C. No Adsorption on Copper Phthalocyanine Functionalized Graphite. *J. Phys. Chem. C* **2014**, *118*, 10076−10082.
(45) Park, J. H.; et al. In-Situ Observation of Initial Stage in Dielectric Growth, and Deposition of Ultrahigh Nucleation Density Dielectric on Two-Dimensional Surfaces. *Nano Lett.* **2015**, *15*, 6626−6633.
(46) Henkelman, G.; Uberuaga, B. P.; Jónsson, H. A Climbing Image Nudged Elastic Band Method for Finding Saddle Points and Minimum Energy Paths. *J. Chem. Phys.* **2000**, *113*, 9901.
(47) Sheppard, D.; Terrell, R.; Henkelman, G. Optimization Methods for Finding Minimum Energy Paths. *J. Chem. Phys.* **2008**, *128*, No. 134106.
(48) Jónsson, H.; Mills, G.; Jacobsen, K. W. In *Nudged Elastic Band Method for Finding Minimum Energy Paths of Transitions*; Berne, B. J.; Ciccotti, G.; Coker, D. F., Eds.; World Scientific: Singapore, 1998; p 385.
(49) Mandeltort, L.; Choudhury, P.; Johnson, J. K.; Yates, J. T. Reaction of the Basal Plane of Graphite with the Methyl Radical. *J. Phys. Chem. Lett.* **2012**, *3*, 1680−1683.
(50) Choudhury, P.; Johnson, J. K. Methyl Chloride Reactions on Lithiated Carbon Nanotubes: Lithium as Both Reactant and Catalyst. *J. Phys. Chem. C* **2011**, *115*, 11694−11700.
(51) Mandeltort, L.; Büttner, M.; Yates, J. T.; Choudhury, P.; Xiao, L.; Johnson, J. K. Carbon−Chlorine Bond Scission in Li-Doped Single-Walled Carbon Nanotubes: Reaction of CH_3Cl and Lithium. *J. Phys. Chem. C* **2010**, *114*, 17148−17158.
(52) Latimer, A. A.; Kulkarni, A. R.; Aljama, H.; Montoya, J. H.; Yoo, J. S.; Tsai, C.; Abild-Pedersen, F.; Studt, F.; Nørskov, J. K. Understanding Trends in C−H Bond Activation in Heterogeneous Catalysis. *Nat. Mater.* **2017**, *16*, 225.
(53) Xu, W.; Apodaca, N.; Wang, H.; Yan, L.; Chen, G.; Zhou, M.; Ding, D.; Choudhury, P.; Luo, H. A-Site Excessive $(La_{0.8}Sr_{0.2})_{1+X}MnO_3$ Perovskite Oxides for Bifunctional Oxygen Catalyst in Alkaline Media. *ACS Catal.* **2019**, *9*, 5074−5083.
(54) Shiota, Y.; Yoshizawa, K. Methane-to-Methanol Conversion by First-Row Transition-Metal Oxide Ions: ScO^+, TiO^+, VO^+, CrO^+, MnO^+, FeO^+, CoO^+, NiO^+, and CuO^+. *J. Am. Chem. Soc.* **2000**, *122*, 12317−12326.
(55) Mowbray, D. J.; Martínez, J. I.; Calle-Vallejo, F.; Rossmeisl, J.; Thygesen, K. S.; Jacobsen, K. W.; Nørskov, J. K. Trends in Metal Oxide Stability for Nanorods, Nanotubes, and Surfaces. *J. Phys. Chem. C* **2011**, *115*, 2244−2252.

https://dx.doi.org/10.1021/acs.jpcc.9b08697
J. Phys. Chem. C 2020, 124, 4502−4510

(56) Ding, X.-L.; Wu, X.-N.; Zhao, Y.-X.; He, S.-G. C−H Bond Activation by Oxygen-Centered Radicals over Atomic Clusters. *Acc. Chem. Res.* **2012**, *45*, 382−390.
(57) Wang, G.; Chen, W.; Huang, L.; Liu, Z.; Sun, X.; Zheng, A. Reactivity Descriptors of Diverse Copper-Oxo Species on ZSM-5 Zeolite Towards Methane Activation. *Catal. Today* **2019**, *338*, 108−116.
(58) Wang, B.; et al. Synthesis and Reactivity of a Mononuclear Non-Haem Cobalt(IV)-Oxo Complex. *Nat. Commun.* **2017**, *8*, No. 14839.
(59) Nam, W. Dioxygen Activation by Metalloenzymes and Models. *Acc. Chem. Res.* **2007**, *40*, 465.
(60) Blakemore, J. D.; Crabtree, R. H.; Brudvig, G. W. Molecular Catalysts for Water Oxidation. *Chem. Rev.* **2015**, *115*, 12974−13005.
(61) Yuan, J.; Zhang, W.; Li, X.; Yang, J. A High Performance Catalyst for Methane Conversion to Methanol: Graphene Supported Single Atom Co. *Chem. Commun.* **2018**, *54*, 2284−2287.
(62) Cui, X.; et al. Room-Temperature Methane Conversion by Graphene-Confined Single Iron Atoms. *Chem* **2018**, *4*, 1902−1910.

https://dx.doi.org/10.1021/acs.jpcc.9b08697
J. Phys. Chem. C 2020, 124, 4502−4510